2.2 THE VENTILATION CLIMATE INFORMATION SYSTEM (VCIS)

S. A. Ferguson,* Steven J. McKay, Trent Piepho, Miriam L. Rorig, Casey Anderson, Lara Kellogg
USDA-Forest Service, Pacific Northwest Research Station, Seattle, Washington

David E. Nagel
USDA Forest Service, Rocky Mountain Research Station, Boise, Idaho

1.0 INTRODUCTION

Air stagnation can enhance the effects of air pollution. Certain aspects of stagnation potential are well known by air pollution managers. For instance, low mixing heights and poor ventilation are common in coastal areas of the United States where moist marine air increases static stability (Holzworth 1972, Holzworth and Fisher 1979). Poor ventilation also is common everywhere at night when radiative cooling at the surface increases atmospheric stability. What is not known, however, is the probability of stagnation on any given day at any selected spot on the landscape. Also, there are few tools that allow stagnation information to be quantitatively assessed across time or space or that allow objective incorporation into land management plans. This is of particular interest to managers of wildland areas in the United States who are responsible for maintaining clean air in Class I areas and for mitigating impacts on air quality and visibility from wildland fires.

To effectively evaluate stagnation potential, we developed the Ventilation Climate Information System (VCIS). The VCIS is comprised of a 40-year time series of wind, mixing height, and a ventilation index at 0000 Universal Time Coordinated (UTC) and 1200 UTC each day. The generated values cover the United States at a horizontal grid spacing of 2.5-minute latitude/longitude (about 5 km), except Alaska where the grid spacing is fixed at 5 km 5 km map projections. The ventilation index is the product of wind speed and mixing height.

We chose to represent stagnation potential with a ventilation index because it is simple to calculate and current and forecast values of ventilation index are well known by air quality regulators and are used for managing biomass smoke in many parts of the country (South Carolina Forestry Commission, 1996; Wade 1989; USDA-Forest Service, Southern Forest Experiment Station 1976; Utah Administrative Code 2001).

Because we needed to generate the high-resolution climate information in a short amount of time, relatively simple tools were used to derive data values and several simplifying assumptions were made. We tried to maintain physical reasonableness, however, and checked our results frequently against observations and common knowledge. Anytime data are derived, however, whether by spatially interpolating observations or physical models, accuracy and reliability are influenced. Therefore, details on the derivation process, assumptions, and methods of smoothing and parameterization are given to help users evaluate uncertainty in subsequent risk assessments.

Complete documentation and summary statistics of the data are in Ferguson et al. (2003) and available from http://www.fs.fed.us/pnw/airfire/vcis. The VCIS website allows users to map monthly values of ventilation index with sensitive receptors, natural and political boundaries, and topography. In addition, users can zoom or print maps. At any time, a summary of daily, monthly, and annual statistics for each variable at any grid point can be obtained by a simple mouse click.

The unique format and robust content of the system has afforded application to wildfire management and prescribed fire planning. We've recently been awarded funding to improve the system and offer a brief summary of its components here to foster dialogue for expanded application.

2.0 SURFACE WIND

To generate surface winds, we modified the single-level hydrostatic flow model of Danard (1977), Dempsey (1985), and Mass and Dempsey (1985). Various versions of the model have successfully simulated sea-land breezes in Israel (Alpert 1988; Alpert and Getino 1988; Alpert et al. 1988), and orographic flow fields for alpine precipitation forecasting (Speers and Mass 1986). We modified the model to accommodate a spatially varying lapse rate and run on a message-passing parallel computing platform. In addition, we modified the finite difference calculations to make them more stable and increase success rate in converging to a physically reasonable solution. We call our modified version of the Danard, Mass, and Dempsey model, WINFLO. We chose to use WINFLO to generate surface winds over the large domain of the United States and the long, 40-year time period because of its rapid computation, reasonably accurate output, and success in a variety of applications.

WINFLO uses sigma coordinates (terrain-following surfaces of constant pressure), with the single-layer sigma surface representing about 10 m above ground level (agl). Only 2 classes of land surface are used, forested land and open water, with drag coefficients of 0.015 and 0.0014, respectively. While we did not find significant differences in model results when we changed the drag coefficient over land during tests in Oregon, we expect that the coarse land-use categories

* Corresponding author: Dr. Sue A. Ferguson, Pacific Wildland Fire Sciences Laboratory, 400 North 34th Street, Suite 201, Seattle, WA 98103. sferguson@fs.fed.us.

may cause the model to underestimate surface winds over broad flat areas and grass lands.

As a hydrostatic model, WINFLO functions best when vertical motions are small compared to horizontal motions. Hydrostatic assumptions typically are inappropriate for horizontal scales less than about 5 km and during strongly dynamic events such as thunderstorms and gusting fronts. To accommodate the hydrostatic assumption, we kept the horizontal grid resolution near 5 km and created an upper limit of 8°C/km and lower limit of 3.5°C/km for the lapse rate. Lapse rates were calculated between the 85 kiloPascals (kPa) and 50 kPa vertical levels. Observed values rarely exceeded 8°C/km but occasionally were less than 3.5°C/km. This forces some smoothing that would cause gusty surface winds to be underestimated by the model. This condition does not affect strong, sustained storm winds that are successfully simulated by WINFLO.

The upper-boundary initialization data were from the National Centers for Environmental Prediction (NCEP) Reanalysis package (Kalnay et al. 1996). We chose to initialize the model with data from the 85 kPa level. This height usually is measured at about 1500 meters above sea level (asl), which is below the height of many mountain ranges in the western United States. At the resolution of the Reanalysis data, however, the western mountains are represented as highly smoothed undulations and the 85 kPa height seems to reasonably represent conditions above major orographic influences while reflecting surface conditions. For example, we simulated winds over the Sawtooth Mountains in Idaho, which consistently rise above 2500 meters asl, with both an 85 kPa reference height and a 70 kPa reference height (about 3000 m asl). When comparing model output with observations, including many high-elevation wind measurements from the interagency RAWS network (U. S. Department of Interior 1995), we found little difference in model performance between the two tests except that the model performed slightly better at turning winds through the terrain patterns when using data from the 85 kPa reference level than when using data from the 70 kPa level. Also, results from the 85 kPa height were consistently better at lower elevation sites.

2.1 Observed vs. Modeled Wind

Surface winds are strongly influenced by small-scale undulations in terrain and land cover. Therefore, wind observations that are measured by anemometers are influenced by, and represent conditions below the resolution of the model terrain and land-use grids and may not represent the larger-scale wind field. In addition, anemometers usually have stall speeds that prevent accurate recording when winds speeds are below about 1 m/s, they can be placed poorly in relation to buildings, towers, and other instruments, and often are poorly maintained. Despite the disconnect between modeled and measured wind values, we compared model output to measurements from the NOAA National Weather Service (NWS) primary observing stations (National Renewable Laboratory 1992; National Climatic Data Center 1997). Data from local and regional networks, such as the interagency RAWS network (United States Department of Interior 1995), did not have adequate quality or consistency for model verification over the entire country and in all seasons.

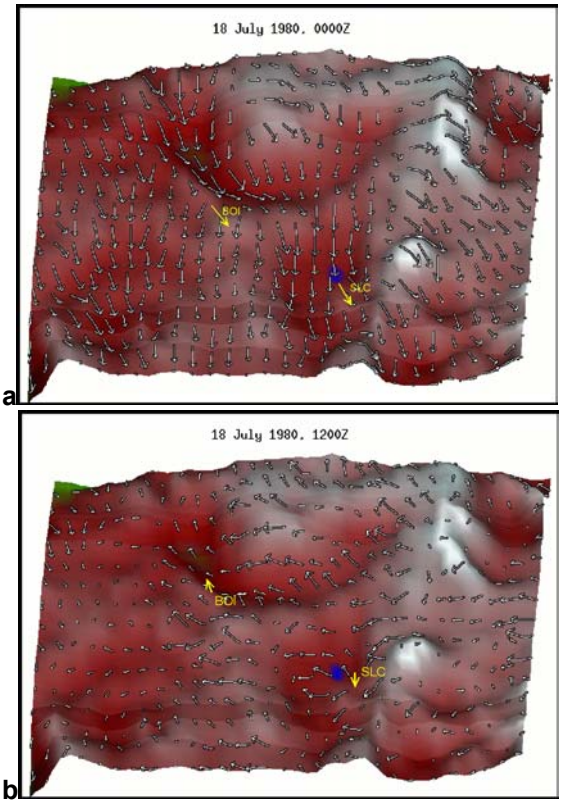

Figure 1. *Modeled surface wind patterns over northern Utah and southern Idaho on 18 July 1980 for a) 0000 UTC and b) 1200 UTC. Observed winds at Salt Lake City, Utah (SLC) and Boise, Idaho (BOI) are shown in yellow.*

Figure 1 illustrates how general flow patterns compare with observations at specific times in a small region centered over southern Idaho and northern Utah. During the afternoon (Figure 1a), observed winds at Boise, Idaho (BOI) and Salt Lake City, Utah (SLC) were from the northwest at about 10 m/s. Modeled winds in the Boise area were generally from the northwest at about 8 m/s but turning north-northeasterly away from the central valley. Modeled winds over Salt Lake City were generally north-northwesterly at about 8 m/s. During the morning (Figure 1b), both modeled and observed winds at Boise became slower and turned southeasterly. While observed winds over Salt Lake City appeared from due north in the morning, modeled winds around the area were variable from southeast to northeast. Away from the observation points, flow patterns appear consistent with typical diurnal wind patterns (up valley during the late afternoon and down valley in the early morning) with expected channel flow through gaps and valleys. Therefore, while minor inconsistencies occur at the observation points, the general flow pattern is physically consistent and realistic. In general we found that WINFLO wind speeds

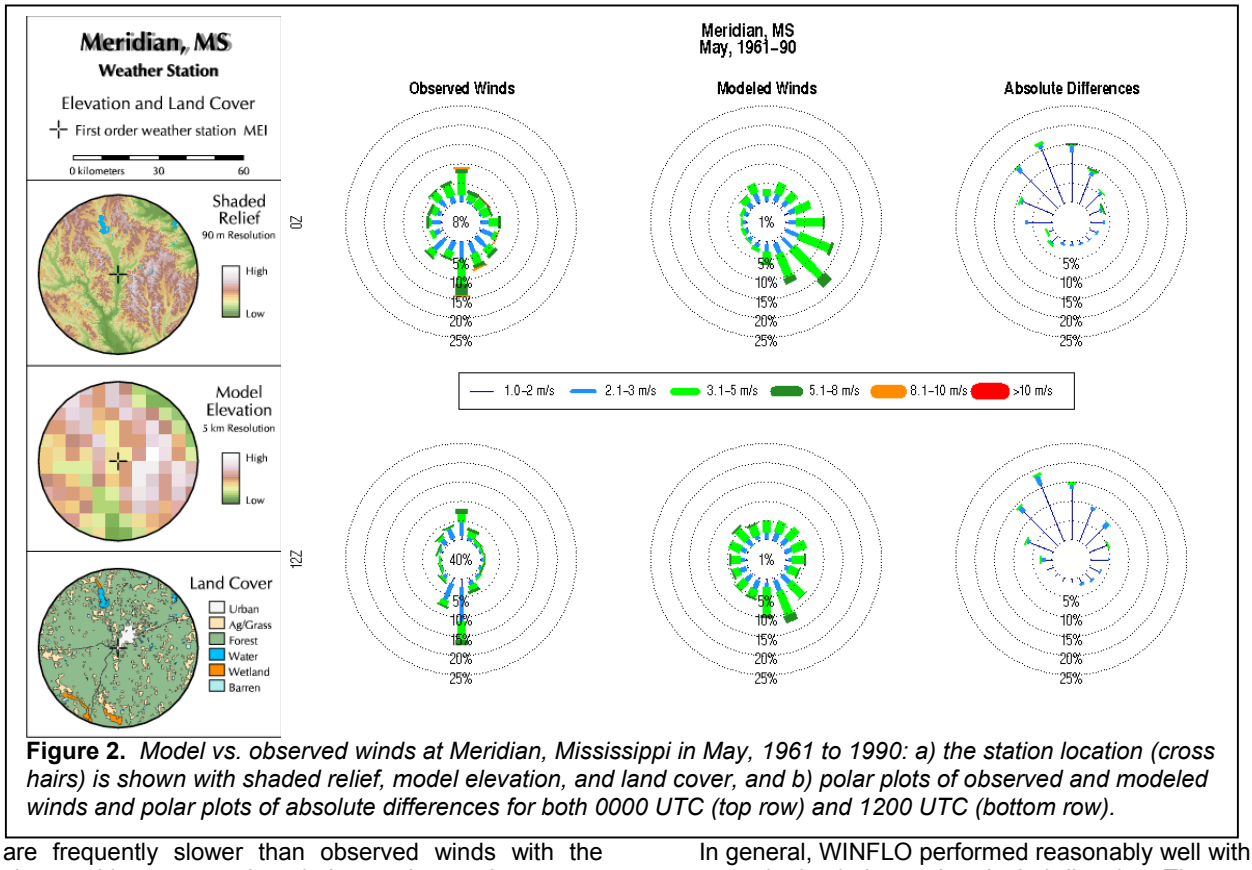

Figure 2. *Model vs. observed winds at Meridian, Mississippi in May, 1961 to 1990: a) the station location (cross hairs) is shown with shaded relief, model elevation, and land cover, and b) polar plots of observed and modeled winds and polar plots of absolute differences for both 0000 UTC (top row) and 1200 UTC (bottom row).*

are frequently slower than observed winds with the slowest biases occurring during spring and summer. This may be due to the inability of the model to capture gusty winds associated with strong convection. When compared to a more fully physical model, such as MM5, the magnitude of errors in speed and direction were similar but WINFLO tends to under predict speed and MM5 tends to over predict (Ferguson et al. 2003).

To help users evaluate errors in their region of interest, we plotted the frequency of modeled and observed wind speed and direction at each observation location (Figure 2). Also included are maps surrounding each observation station that show the 90-meter resolution terrain, model terrain at 2.5′ latitude-longitude or 5km resolution, and land use at 90-meter resolution. This allows the user to distinguish whether differences between modeled and observed winds at that location are due to smoothing of terrain and land-use in the model or caused by the model physics. On the polar difference plots, the line thickness indicates the magnitude of difference in speed and the line orientation shows the angle of difference in direction. A zero difference in direction would appear as a line pointing from zero degrees straight up and a zero difference in speed is represented by a thin line. For example, at Meridian, MS (Figure 2) the modeled wind speed is most often the same as observed but is commonly 10 to 20 degrees different in direction (observed winds are southerly while modeled winds are southeasterly). The difference in direction appears to be due to the narrow valley that influences winds at Meridian, which is not resolved by the model topography.

In general, WINFLO performed reasonably well with respect to both wind speed and wind direction. The two land-use categories (land and water) in the model, however, tend to bias toward rough terrain (forested and mountainous). This causes strong winds (> 8 m/s) to be underestimated over broad flat areas and grass lands. Also, the smoothed model terrain appears to cause a modest directional bias of less than 45°. Finally, restrictions on the model lapse rate (temperature difference with height) and lack of radiative heating appear to cause poor model performance in some months at western arid sites.

3.0 MIXING HEIGHT

Because the NCEP Reanalysis data are at a relatively coarse vertical resolution, they cannot be used to accurately determine mixing heights. Therefore, mixing heights are determined from radiosonde observation (RAOB) data. To derive mixing heights, we lift a parcel of air adiabatically from the surface with a starting temperature near the maximum or minimum daily temperature as described in Holzworth (1972). The mixing height is defined as that level where the temperature of the adiabatically lifted parcel becomes less than the measured ambient temperature. Once this occurs, it is assumed that the parcel, being cooler than its surroundings, will reach neutral buoyancy and stop rising.

The calculated mixing heights are interpolated between RAOB sites using the Cressman scheme

(1959) as described in (Manning and Haagenson 1992). Frontal boundaries between air masses are not considered, partly because they are difficult to determine automatically from archived data, and also because we assume that their exact position is not critical in a climatological assessment of mixing height. Thus mixing height is mapped to smoothly vary over the landscape except on calm, clear nights when the morning mixing height is modified by local inversions (Section 3.1) and where interpolated mixing heights intersect higher terrain (Section 3.2).

3.1 Local Inversion Potential

At night, in addition to the stabilization of air and lower mixing height, down-slope winds and terrain features can cause cooling air to be trapped in stagnant pools forming patterns of local temperature inversions in places well away from and poorly represented by RAOBS. These areas also can trap smoke and other pollutants. Currently there is no meteorological model that can adequately simulate the timing and location of local inversions on a national scale. Therefore, we created a set of algorithms that determine the occurrence, location, and strength of local temperature inversions based on climate records of nearby surface weather stations and terrain features.

To determine the occurrence potential of a local inversion, a set of criteria were adapted from Pasquill (1962) and Turner (1964) who describe the formation of a surface-based temperature inversion as dependent on surface wind speed and net long-wave radiation leaving the lowest layer of the atmosphere, which depends on cloud cover. Hourly values of wind speed, total cloud cover, opaque cloud cover, and present weather (defined as fog, drizzle, rain, snow, etc.) (National Renewable Energy Laboratory 1992; National Climatic Data Center 1997) are used to determine whether a stable surface layer will form. The potential for a local inversion to occur is initiated if the following criteria are met for at least 50% of all reported hours between 1800 and 0600 local time:

- Wind speed is ≤ 3 m/s, total cloud cover is ≤ 8/10, and opaque cloud cover is ≤ 6/10, or
- wind speed is > 3 m/s but ≤ 5 m/s, the total cloud cover is ≤ 6/10 and opaque cloud cover is ≤ 3/10; or
- if fog has been reported at any hour between 1800 and 0600 local time.

On nights with excessive missing data, no inversion is expected if there are more than two reports of winds exceeding 5 m/s. If all reported winds are less than 5 m/s, then the available hours of cloud cover determine inversion potential.

Criteria for the occurrence of a local inversion were checked at all available surface stations then applied to grid cells in the surrounding neighborhood (Figure 3). If a surface-based inversion were determined to occur at the observing station then all grid cells within the neighborhood also were assumed to have a local inversion potential.

Figure 3. *Neighborhoods for determining local inversion potential in the contiguous United States. Letters indicate the NWS identifier for the station that was used to determine calm, clear conditions within the neighborhood.*

To locate and rank potential local inversions, a GIS algorithm was developed to identify terrain features that promote the collection and trapping of subsiding air:

1. Height is vertically exaggerated by 5 times. This helps to highlight shallow **valleys and hollows** that are difficult to resolve with 5-km grid cells.

2. Flat areas are defined by slope that is less than 0.8º and, to eliminate insignificant flat areas, a 3-pixel by 3-pixel smoothing filter is applied.

3. Valleys and basins are defined by negative curvature, which is smoothed with a one-cell radial filter.

4. Flow accumulation is computed for areas exceeding 17 pixels. The 17-pixel threshold is chosen subjectively to eliminate flow potential that crosses ridgelines or begins at mountaintops. With a 5-km grid size, the threshold is 425 km^2.

5. Because not all places of negative curvature (e.g., benches) will form a local inversion, potential areas of drainage accumulation are defined by places where lines of **flow accumulation intersect valleys and basins**.

6. Because not all flat places will form a local inversion (e.g., plateaus), potential areas of pooling are defined by places where lines of **flow accumulation intersect flat areas**.

The resulting map of potential inversion locations in the example domain is shown in Figure 4.

We derived values of strength to help map inversion heights by assuming that the potential strength of local inversions is correlated to the amount of accumulated flow. In general, as flow accumulation increases downstream, so does the inversion strength. Strength values increase rapidly as rivers join and when flow is contributed from different watersheds. By superimposing flow accumulation on the inversion potential map, we derived inversion strength values that ranged from 0 to 11589, with over 95% of the grid cells having a value less than or equal to 366.

To determine the height above ground, we applied a logarithmic function:

$$H = 25.2430 \times \ln\left[S_t \times 1.0404\right],$$

where H is the inversion height (m agl) and S_t is the inversion strength truncated below 366. By bounding the inversion strength values below 366 (i.e., all values above 366 were given a value of 366) we keep the inversion height from exceeding 150 m agl, the typical height of nighttime surface-based inversions.[2]

The vast majority of major valleys have inversion strengths less than 366. For example, the Bitterroot Valley in Montana has an inversion strength of about 40, giving it an inversion height of 94 m agl at the valley bottom. The Snake River Valley in Idaho and the mouth of the Columbia River in Oregon have inversion strengths of about 618 and 7000, respectively. Because both are greater than 366, their potential inversion height at valley bottom is 150 m agl Note that inversion heights decrease toward the head of the valley. This allows a somewhat smooth transition between areas with a local inversion and areas without a local inversion.

There are very few direct observations of local inversion occurrence or location. At RAOB locations, where surface-based inversions can be directly measured, we tested our inversion occurrence criteria and found that observed, surface-based inversions occurred on nearly all days that the criteria of calm wind and clear skies were met. A surface-based inversion was determined to exist if the 1200 UTC RAOB included two adjacent layers within 1000 meters of the surface that reported warmer air over cooler air. No distinction was made between inversion strength or depth.

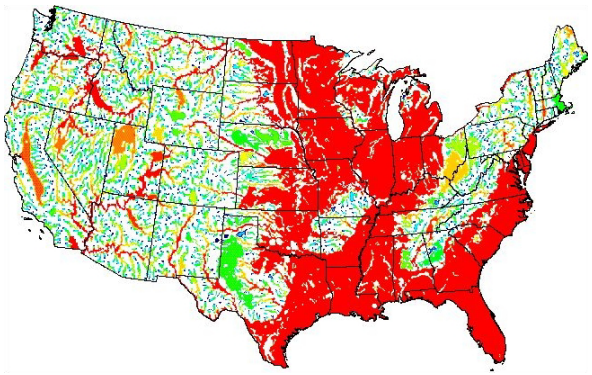

Figure 4. *Inversion location and relative depth. Red colors indicate maximum flow accumulation with depths near 150 m agl and blue colors indicate minimum flow accumulation. White indicates places where terrain configurations are not expected to influence the formation of local inversions.*

Unfortunately, RAOBS are sparsely distributed over the United States. Additionally, these stations are typically located in flat areas or broad valleys where local inversions are less significant than in narrow valleys, small hollows, and basins that are typical of wildland areas. Therefore, most of our verification techniques for local inversion potential are qualitative in nature. When compared with satellite observations of morning fog and smoke, patterns appear reasonably similar. For example, Figure 5 shows an image from the

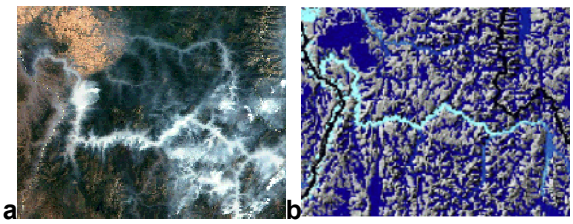

Figure 5. *(a) Observations of smoke over central Idaho at about 10am in July 2000. (b) Map of inversion potential with light blue showing strongest potential and dark blue showing weaker potential.*

Moderate Resolution Imaging Spectrometer (MODIS) satellite image over the Salmon River in central Idaho during the 2000 wildfires along with a map of local inversion potential for the same general area. From the satellite image (Figure 5a), it appears that most smoke is concentrated in the Salmon River valley, where the strongest inversion potential is indicated by light blue (Figure 5b). Darker blue colors indicate potential inversions in side valley and tributaries, where the satellite image shows more transparent smoke concentrations.

3.2 Adjusted Mixing Height

The local inversion algorithm was applied to morning (1200 UTC) mixing heights only and only to grid cells in the neighborhood of a surface observation showing calm winds and clear skies the previous night. Grid cells not in a terrain feature that fosters the development of a local, nighttime inversion (i.e., peaks, ridges, plateaus, etc.) are assumed to be experiencing the ambient condition of mixing heights interpolated from RAOB measurements.

There are times when the measured mixing height passes below ground level as it is interpolated across the landscape. This happens frequently when the mixing height is relatively low, such as during a winter morning, or in places where mountains are between RAOB locations. At these times and in these places, above the interpolated mixing height, air parcels often are free to lift to great heights, occasionally reaching the tropopause. In an attempt to approximate the "free-atmosphere" mixing depth, we arbitrarily assigned a value of 4000 m agl in the afternoon and 1000 m agl in the morning, which coincide with highest measured heights at those times (Holzworth 1972). Currently, we are improving this approximation by calculating boundary-layer heights above the surface mixing depth from observed values at each time step.

Figure 6 shows the effect of adjusted mixing heights on a July morning when the local inversion potential is imposed. Note that valley inversions become visible in the northwestern United States and in the Appalachian Mountains after the inversion algorithm is imposed.

[2] Holzworth and Fisher (1979) found that nearly all surface-based inversions were at least 100 m deep.

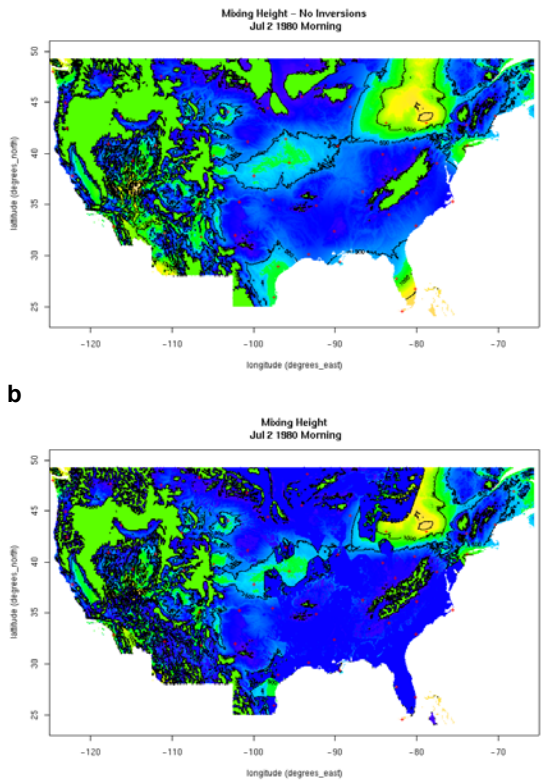

Figure 6. *Interpolated mixing height for the morning of July 1, 1980 (a) without adjustment for local inversion, and b) with local inversions. Blue colors indicate lowest heights and yellow colors indicate highest heights.*

4.0 VENTILATION INDEX

The ventilation index is the product of wind speed and mixing height. In most cases, the index uses the average value of wind speed in the mixed layer or a local steering wind, which often is well above 10 meters, the height of wind derived for this study. Also, we have modified the mixing height to account for local inversions. The local inversion correction creates lower values of ventilation potential at remote sites, which is more applicable than indexes calculated from a central RAOB location. Therefore, values of ventilation index in VCIS are relatively conservative and may best be applied to smoke concerns relatively close to the ground.

To map index values in a meaningful way and help assess the values of air quality and visibility that are at risk, we followed a common procedure of classifying the ventilation index into categories of poor, marginal, fair, and good. We assigned a classification scheme that is half of commonly used classes (Leenhouts et al. 2001), however, because wind speeds at 10 m agl typically are about half of those at 40 m agl, which is closer to the height of a trajectory wind. The resulting classification scheme is summarized in Table 1.

Table 1. Classification of ventilation potential from ventilation index values in the VCIS database.

Ventilation Index (m^2/s)	Classification
0-1175	Poor
1176-2350	Marginal
2351-3525	Fair
>3525	Good

Figure 7 illustrates the monthly mean classifications of ventilation index for October in the 48 contiguous states. Note the large areas of relatively poor ventilation potential in low-lying areas during the morning. During the afternoon, the ventilation potential improves dramatically. Marginal conditions prevail, however, in the lee of several western mountain ranges.

Monthly mean maps of the ventilation index classes are available on the VCIS website for all months and all 50 states. The interactive website allows users to plot sensitive receptors, such as hospitals, schools, airports, wilderness areas, and highways as overlays on the ventilation index maps. In addition, users can zoom, pan, add elevation contours, cities, state and county boundaries, and rivers and railroads to help exactly locate areas of potentially high risk.

To help determine the timing of poor or good stagnation conditions, year-to-year and day-to-day time series have been generated for each grid point. The time series include the median (50th percentile), quartiles (25th and 75th percentiles), and extreme values (maximum and minimum) for each day of a given month or each month of a given year. For example, Figure 8 shows the variation of ventilation potential for a grid point in Georgia during the afternoon in April. At this location, in this month, and at this time of day, the ventilation index generally is fair, often marginal, and with periods of poor and good ventilation. The left side of the figure illustrates the variability within each day of the month across multiple years. The right side illustrates the variability within the month from year to year. Color bars on axes show that most of the ventilation index values occur in the marginal to fair range at this site in April.

5.0 CONCLUSION

VCIS assists users in assessing values of air quality and visibility at risk from wildland fire and other sources of pollution by illustrating the spatial and temporal variability of ventilation potential. The 40-year, twice-daily time series at 2.5' latitude-longitude and 5-km spatial resolution can be viewed as monthly averaged maps of index classifications or in plots of frequency and magnitude at user-selected grid points.

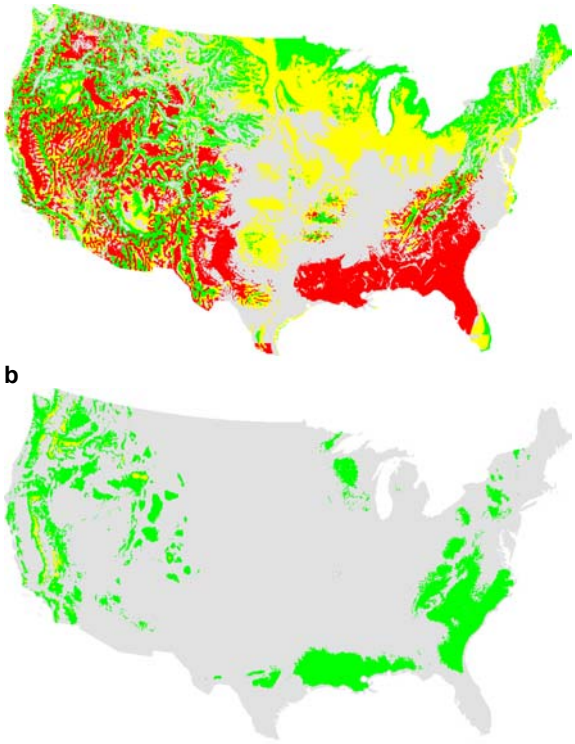

Figure 7. *Monthly mean maps of ventilation index classifications for a) morning and b) afternoon in October. Red represents potentially poor ventilation conditions, yellow is marginal, green is fair, and gray is good.*

The ArcIMS web-access system allows users to view local to national patterns of ventilation potential. Overlays of sensitive receptors (hospitals, schools, roads, airports, etc.) help quantify the proximity of risk to poor ventilation conditions.

Despite some of the smoothing and simplifying assumptions required to generate such a large, national data set, the spatial values provide a reasonably accurate view of ventilation potential and associated risks to air quality and visibility in the United States.

Because VCIS offers the first historical perspective of ventilation potential and associated risks to air quality and visibility at a high spatial and temporal resolution on a national scale, the information it holds about patterns and probabilities of risk are just beginning to be explored. During summer and fall of 2002, the system was used to help anticipate potential smoke impacts from the long-smoldering Biscuit wildfire in southwestern Oregon. It was used to help justify a smoke management plan in central Idaho and to illustrate management alternatives in NEPA documentation for a project in Colorado.

As we embark on improving the system, we hope to increase spatial resolution, include calculations of frequency to determine how often values reach user-defined threshold criteria, and improve physical and numerical methods of generating the spatial values.

6.0 ACKNOWLEDGEMENTS

This project was funded through generous support of the Joint Fire Science Program (U.S. Department of Interior and USDA Forest Service). The authors gratefully acknowledge the advice and assistance of Shokoofey Nowbakht and David Dempsey (San Francisco State University) in modifying early versions of the WINFLO model to incorporate spatially varying lapse rates. Our method of defining the location of local inversions is based on a concept suggested by Dr. Jan Henderson (USDA Forest Service, Region 6). Special thanks to Steven Hostetler, Rich Fisher, Narasimhan Larkin, and David V. Sandberg for their thoughtful reviews.

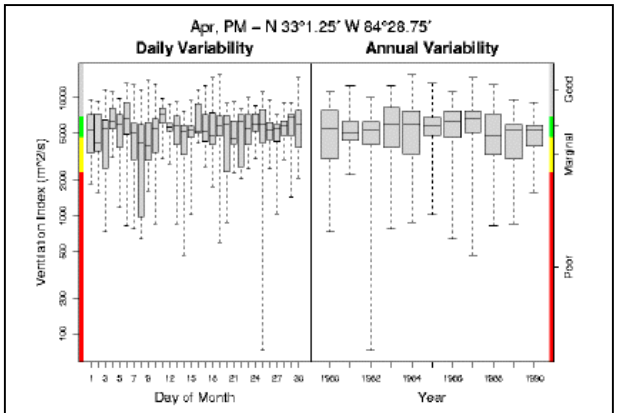

Figure 8. *Box plot of ventilation index for a site in Georgia during the afternoon in April. Boxes show 25th and 75th percentile. Whiskers show extreme values. Median is indicated by horizontal line in each box. Color bars on each axis indicate poor, marginal, fair, and good classification values (Table 1).*

7.0 REFERENCES

Alpert, P.; Getenio, B.; Zak-Rosenthal, R. 1988. One-level modeling for diagnosing surface winds over complex terrain: II. applicability to short-range forecasting. Monthly Water Review. 116(10): 2407-2461.

Alpert, P.; Getenio, B. 1988. One-level diagnostic modeling of mesoscale surface winds in complex terrain: I. comparison with three-dimensional modeling in Israel. Monthly Weather Review. 116(10): 2025-2046.

Alpert, P. 1988. The combined use of three different approaches to obtain the best estimate of meso-surface winds over complex terrain. Boundary-Layer Meteorology. 45: 291-305.

Cressman, G.P. 1959. An operational objective analysis system. Monthly Weather Review. 87: 367-374.

Danard, M. 1977. A simple model for mesoscale effects of topography on surface winds. Monthly Weather Review. 105: 572-580.

Dempsey, D.P. 1985. A one-level mesoscale model for diagnosting surface winds in mountainous and coastal regions. University of Washington. Ph.D. dissertation.

Ferguson, S.A., S.J. McKay, D.E. Nagel, T. Piepho, M.L. Rorig, C. Anderson, L. Kellogg. 2003. Assessing values of air quality and visibility at risk from wildland fires. U.S. Department of Agriculture, Forest Service, Pacific Northwest Research Station, Research Paper PNW-RP-550, 59 pp.

Leenhouts, B., C.C. Hardy, R.D. Ottmar, J.L. Peterson, J.E. Core, and P. Seamon, editors. National Wildfire Coordinating Group, National Interagency Fire Center, Great Basin Cache Supply Office, Boise, ID. NFES #1279.

Holzworth, G.C. 1972. Mixing heights, wind speeds, and potential for urban air pollution throughout the contiguous United States. Office of Air Publication No. AP-101. Research Triangle Park, NC: United States Environmental Protection Agency, Office of Air Programs.

Holzworth, G.C.; Fisher, R.W. 1979. Climatological summaries of the lower few kilometers of rawinsonde observations. United States Environmental Protection Agency, Office of Research and Development, Research Triangle Park, North Carolina. 140 pp.

Kalnay, E.; Kanamitsu, M.; Kistler, R.; Collins, W.; Deaven, D.; Gandin, L.; Iredell, M.; Saha, S.; White, G.; Woollen, J.; Zhu, Y.; Chelliah, M.; Ebisuzaki, W.; Higgins, W.; Janowaik, J.; Mo, K.C.; Ropelewski, C.; Wang, J.; Leetmaa, A.; Reyholds, R.; Jenne, R.; Joseph, D. 1996. The NCEP/NCAR 40-year reanalysis project. Bulletin of the American Meteorological Society. 77(3): 437-471.

Manning, K.W.; Haagenson, P.L. 1992. Data ingest and objective analysis for the PSU/NCAR modeling system: Programs DATAGRID and RAWINS. NCAR Technical Note NCAR/TN-376+IA. [Boulder, CO]: [National Center for Climate Research]. 209 pages.

Mass, Clifford F.; Dempsey, David P. 1985. A one-level, mesoscale model for diagnosing surface winds in mountainous and coastal regions. Monthly Weather Review. 113:1211-1227.

National Climatic Data Center. 1997. Hourly United States weather observations 1990-1995. National Climatic Data Center, 151 Patton Avenue, Asheville, NC 28801 and United States Environmental Protection Agency, Research Triangle Park, Raleigh, NC.

National Renewable Laboratory. 1992. National solar radiation data base 1961-1990. Volume I, II, and III. National Climatic Data Center, Federal Building, Asheville, NC, 28801.

Pasquill, F. 1962. Atmospheric diffusion. London: Van Nostrand. 209.

South Carolina Forestry Commission. 1996. Smoke Management Guidelines for Vegetative Debris Burning Operations: State of South Carolina. SCFC 3rd Printing. 19 pp.

Speers P.; Mass, C.F. 1986. Diagnosis and prediction of precipitation in regions of complex terrain. WSDOT Final Report WA-RD-91.1. Washington State Department of Transportation, Transportation Building, Olympia, WA 98504. 166 pp.

Turner, D. B., 1964. A dispersion model for an urban area. Journal of Applied Meteorology. 3: 83-91.

U. S. Department of the Interior. 1995. Remote Automated Weather Stations (RAWS) and Remote Environmental Monitoring Systems (REMS) Standards for the United States Department of the Interior, Bureau of Land Management. Boise, ID: Bureau of Land Management; National Fire Information Center.

USDA Forest Service, Southern Forest Experiment Station. 1976. Southern forestry smoke management guidebook. United States Department of Agriculture, Forest Service, Southern Forest Experiment Station. SE-10. 55 pp.

Utah Administrative Code. 2001. Emission standards: General Burning. R307-202. Michael G. Broschinsky, Administrative Code Editor, Division of Administrative Rules, PO Box 141007, Salt Lake City, Utah 84114-1007.

Wade, D.D. 1989. A Guide for prescribed fire in southern forests. National Wildfire Coordinating Group, Prescribed Fire and Fire Effects Working Team, Boise Interagency Fire Center, ATTN: Supply, 3905 Vista Avenue, Boise, ID 83705. NFES #2108. [United States Department of Agriculture, Forest Service, Southeastern Forest Experiment Station. Tech. Pub. R8-TP 11.] 56 pp.